Spin-orbit coupling effects in two-dimensional circular quantum rings: Elliptical deformation of confined electron density

M. P. Nowak and B. Szafran
Faculty of Physics and Applied Computer Science, AGH University of Science and Technology, al. Mickiewicza 30, 30-059 Kraków, Poland

(Received 2 October 2009; published 23 November 2009)

We study electron states confined in two-dimensional circular quantum rings in the presence of spin-orbit coupling due to both structure and crystal inversion asymmetry in the external magnetic field. It is demonstrated that the confined electron density loses the circular symmetry of the confinement potential provided that both Rashba and Dresselhaus coupling constants are nonzero, with the exception of a special case of equal coupling constants and absence of the spin Zeeman interaction. An elliptical deviation from the circular symmetry—present already for a single confined electron—is for two electrons strengthened by the Coulomb repulsion. We discuss signatures of the charge-density deformation in the experimentally accessible quantities: magnetization and charging properties of the ring. Relevance of the results of one-dimensional ring models for description of spin-orbit coupling effects is also discussed.

DOI: 10.1103/PhysRevB.80.195319 PACS number(s): 73.40.Gk, 73.21.Hb

I. INTRODUCTION

Spin-orbit coupling in semiconductor nanostructures is considered useful for spintronics and quantum information processing since it translates the spatial motion of an electron into rotation of its spin.[1–6] In quantum dots the spin-orbit coupling[7–14] leads to decay of confined electron spin polarization.[15] Spin-orbit-coupled open quantum rings and their arrays are studied in the context of the Aharonov-Casher effect[16,17] and other spin-related transport phenomena[18–21] as well in quantum gates design.[5] Persistent currents in closed semiconductor quantum rings attracted a lot of theoretical attention[22–31] and the interest in this field is renewed by the recent observation of the magnetization produced by self-assembled quantum rings.[32] The effect of spin-orbit coupling on the magnetization, persistent spin, and charge currents in closed quantum rings[33–39] was extensively studied within strictly one-dimensional approximations of the ring confinement.

The spin-orbit interaction in semiconductor nanostructures—although crucial for spin manipulation and relaxation—has energetically weak effects. In particular for quantum rings the spin-orbit coupling energy is by at least two orders of magnitude smaller than the energy spacing between the ground and the first-excited states of radial quantization. This fact is usually accepted as a natural argument for strictly one-dimensional approximations[33–40] in the discussion of the spin-orbit coupling effects. The one-dimensional models are based on an effective energy operator derived by averaging the actual Hamiltonian with the ground-state radial wave function.[39]

In the present paper we perform a systematic exact diagonalization study of one and two electrons confined in two-dimensional circular quantum rings in the presence of the spin-orbit coupling due to the inversion asymmetry of both the structure (Rashba coupling) and the crystal lattice (Dresselhaus coupling). The exact diagonalization results are confronted with the ones produced by the lowest-radial-state approximation, which turns out to introduce a number of artificial effects in the spectra and charge densities of the confined system, particularly when both spin-orbit coupling types are present. The case of comparable contributions of the Dresselhaus and the Rashba types of coupling is the one for which persistent helical spin densities waves appear in the two-dimensional electron gas.[41,42]

In the presence of spin-orbit coupling the stationary states—even when confined in circular potentials—are no longer orbital angular-momentum eigenstates. However, when only a single type of the coupling—Rashba or Dresselhaus—is present both the spin-up and spin-down components of the wave function do have definite angular momenta, and in consequence the spin and charge densities retain the circular symmetry of the confinement potential. When both types of the spin-orbit interaction are simultaneously present the spin densities lose the circular symmetry, and thus a possibility of deviation of the charge density from the circularity is also opened. Indeed such a pronounced deformation of the charge density was found in Ref. 34, in particular for equal Rashba and Dresselhaus coupling constants and in the absence of the Zeeman spin interaction. We identify this result as an artifact of the lowest-radial-state approximation. The deformation of the charge density is indeed found in two-dimensional rings but only in the presence of the spin Zeeman effect and/or for nonzero but unequal coupling constants. Moreover, the actual deformation occurs in a perpendicular direction to the one predicted by the lowest-radial-state approximation. We demonstrate that the charge-density deformation distinctly influences experimentally accessible ground-state properties including the chemical potential which determines the single-electron charging of the ring[43] and the magnetization[32] produced by persistent currents, especially for two electrons for which the deformation is radically enhanced by the Coulomb interaction.

II. THEORY

We consider a two-dimensional single-electron Hamiltonian with the magnetic field perpendicular to the plane of confinement

$$h = \left(\frac{\mathbf{p}^2}{2m^*} + V(r) \right) \mathbf{1} + \frac{1}{2} g \mu_B B \sigma_z + H_R + H_D, \quad (1)$$

where $\mathbf{p} = -i\hbar\nabla + e\mathbf{A}$, the vector potential is taken in the symmetric gauge $\mathbf{A} = B(-y/2, x/2, 0)$, $\mathbf{1}$ is the identity matrix, $V(r)$ stands for the confinement potential, and H_R and H_D introduce the linear Rashba and Dresselhaus spin-orbit interactions. For x and y axes oriented parallel to [100] and [010] crystal directions, respectively, the spin-orbit terms have the form

$$H_R = \alpha(p_y\sigma_x - p_x\sigma_y)/\hbar \quad (2)$$

and

$$H_D = \beta(p_x\sigma_x - p_y\sigma_y)/\hbar. \quad (3)$$

The two-dimensional Dresselhaus coupling constant $\beta = (\frac{\pi}{d})^2 \beta_{3D}$ depends on d—the thickness of the layer of confinement in the growth direction—and the bulk Dresselhaus constant β_{3D}. For the most popular value of GaAs bulk constant[44] $\beta_{3D} = 27.5$ eV Å^3 and $d = 5$ nm one has $\beta = 10.8$ meV nm, which is used below as the maximal realistic value (for the alloyed InGaAs material constant β_{3D} is slightly increased[45]). The value of the Rashba constant α depends on the slope of the potential along the growth direction, which is partially defined by the growth conditions (asymmetric doping or indium concentration profile) but can be tuned by electrical gating,[46] in particular to match the Dresselhaus coupling constant for observation of the helical spin-density waves.[41,42]

We consider a circular quantum ring potential

$$V(r) = -V_0\{\exp[-(r/R_o)^\gamma] - \exp[-(r/R_i)^\gamma]\} \quad (4)$$

and apply parameters corresponding to etched $In_{0.1}Ga_{0.9}As/GaAs$ quantum rings:[47] potential depth $V_0 = 50$ meV, electron effective mass $m^* = 0.063m_0$, dielectric constant $\epsilon = 13.125$, and Landé factor $g = -2.15$. We assume the outer and inner ring radii of $R_o = 60$ nm and $R_i = 40$ nm, respectively. In Eq. (4) we apply parameter $\gamma = 35$, for which the radial potential is close to a rectangular quantum well.

The spectrum for the single electron without spin-orbit coupling is given in Fig. 1. The ground-state angular-momentum transitions occur nearly ideally periodically, which is a characteristic feature of nearly one-dimensional rings. The magnetic period of the ground-state Aharonov-Bohm oscillation is 0.565 T, which corresponds to a flux quantum threading a strictly one-dimensional ring of radius $R_{1D} = 48.3$ nm. In Fig. 1 more or less 25 meV above the ground state we observe a branch of energy levels corresponding to the first radial excitation.

For $\beta = 0$ ($\alpha = 0$) Hamiltonian (1) commutes with the total angular momentum J_+ (J_-) operator defined as $J_\pm = L_z \pm S_z$, where $S_z = \frac{\hbar}{2}\sigma_z$ is the operator of the z component of the spin and $\mathbf{L} = -i\hbar\mathbf{1}(\mathbf{r} \times \nabla)$ is the orbital angular-momentum operator. For a single type of the spin-orbit coupling present the single-electron Hamiltonian eigenstates are therefore of the form

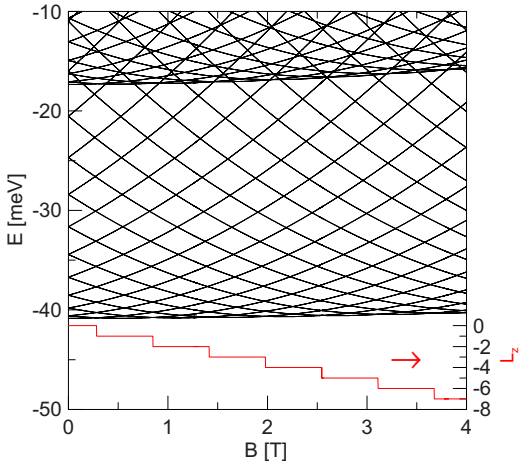

FIG. 1. (Color online) Single-electron energy spectrum for the ring defined by Eq. (4) without spin-orbit coupling. The red line near the bottom of the plot shows the ground-state angular momentum.

$$\psi = \begin{pmatrix} \psi_{l_\uparrow}(r)\exp(il_\uparrow\phi) \\ \psi_{l_\downarrow}(r)\exp(il_\downarrow\phi) \end{pmatrix} \quad (5)$$

with $l_\downarrow = l_\uparrow + 1$ for the Rashba and $l_\downarrow = l_\uparrow - 1$ for the Dresselhaus coupling. When both types of the spin-orbit coupling are present the Hamiltonian still commutes with the s-parity operator $P_s = P\sigma_z$, where P is the scalar parity operator $[Pf(\mathbf{r}) = f(-\mathbf{r})]$. The spin-up and spin-down components of the Hamiltonian eigenstates possess opposite parities.

The single-electron spin orbitals are found by diagonalization of the Hamiltonian in a basis of multicenter Gaussian functions[48]

$$\psi_\nu = \sum_{ks} c_{ks}^\nu \chi_s \exp\left[-\frac{(\mathbf{r} - \mathbf{R}_k)^2}{2a^2} + \frac{ieB}{2\hbar}(xY_k - yX_k) \right], \quad (6)$$

where summation over k runs over centers of Gaussians $\mathbf{R_k} = (X_k, Y_k)$, $s = \pm 1$ and χ_s are eigenstates of the Pauli matrix σ_z. In Eq. (6) integer ν numbers the Hamiltonian eigenstates. The imaginary term in the exponent is due to the magnetic translation which ensures equivalence of all the centers in the presence of the external magnetic field. The centers $\mathbf{R_k}$ are distributed on a square array[48] of 31×31 centers spaced by $\Delta x = \Delta y = 5.2$ nm. We use the basis function localization parameter a equal to the variationally optimal value of 5.7 nm.

The two-electron eigenproblem for the Hamiltonian $H = h(1) + h(2) + (e^2/4\pi\epsilon\epsilon_0 r_{12})$ is diagonalized in the basis of antisymmetrized products of operator (1) eigenstates,

$$\Psi = \frac{1}{\sqrt{2}} \sum_{\mu=1}^{K} \sum_{\nu=\mu+1}^{K} [\psi_\mu(1)\psi_\nu(2) - \psi_\mu(2)\psi_\nu(1)]. \quad (7)$$

Convergence of the calculation up to 0.01 meV is usually reached for $K = 22$, and the present approach allows for inclusion of up to at least $K = 52$ single-electron states. Typically, the difference between the two-electron energies as calculated for 52 and 22 single-electron basis states is smaller than 1 μeV. Discussion of the applicability of the

multicenter basis to the two-electron problem is given in Ref. 48.

III. RESULTS AND DISCUSSION

The presentation of the results is organized in the following way. First we consider the single-electron states in the absence of the Zeeman interaction ($g=0$). We begin by the case of a single type of the spin-orbit coupling present (Sec. III A), then we discuss the symmetry breaking as found in the lowest-radial-state approximation for $\alpha=\beta$ (Sec. III B), the case of nonzero but not-equal coupling constants is discussed in Sec. III C. In Sec. III D the effects of the Zeeman interactions are explained. The two-electron states are discussed in Sec. III E. Results for magnetization and chemical potentials are provided in Sec. III F.

A. $\beta=0$, $g=0$,

Red (dashed) lines in Fig. 2(a) show the energy spectrum for a single type of the spin-orbit coupling present—pure Dresselhaus or pure Rashba case. In Fig. 2(b) we additionally plotted the J quantum number (eigenvalue of the total angular-momentum operator J_z), the average values of the orbital angular momentum (both expressed in $\hbar$), and the z component of the spin (in $\hbar/2$ units). Figure 2(b) was produced for the pure Rashba coupling—for the Dresselhaus coupling J and $\langle L\rangle$ values stay the same, but the average value of the z component of the spin is inverted. With the black lines in Fig. 2(a) we plotted the results of the analytical formula[18] for the pure Rashba coupling spectrum within the one-dimensional approximation

$$E_l^s = \frac{\hbar\omega_0}{2}\left\{\left[\left(n'+\frac{1}{2}\right)^2+\frac{1}{4}\right]+s\left(n'+\frac{1}{2}\right)\sqrt{1+\left(\frac{\omega_R}{\omega_0}\right)^2}\right\}, \tag{8}$$

where $\omega_0=\hbar/(m^* r_0^2)$, $\omega_R=2\alpha/(\hbar r_0)$, $n'=l+\Phi/\Phi_0$, $l=0,\pm1,\pm2,\ldots$ and $s=\pm1$ are the angular momentum and spin quantum numbers, respectively, r_0 is the effective radius of the ring, Φ is the magnetic flux threading the ring, and Φ_0 is the flux quantum. The results of Eq. (8) as given in Fig. 2 were obtained for $r_0=R_{1D}=48.3$ nm in consistence with the average ring radius estimated above from the period of the ground-state Aharonov-Bohm oscillation of Fig. 1. The results of the one-dimensional formula (8) were shifted on the energy scale by −40.94 meV to coincide with the two-dimensional results for $B=0$. As B grows the energy as obtained in the two-dimensional model rise due to the diamagnetic effect, absent for strictly one-dimensional rings. Moreover, we notice that avoided crossings are opened in the exact spectrum above the ground state. For instance near $B=2$ T there is an avoided crossing between the second- and third-excited energy levels, which both correspond to $J=-3.5$ and differ by the majority-spin orientation [this can be noticed by inspecting $\langle S_z\rangle$ in Fig. 2(b) when they become ground states, i.e., near 1.5 and 2.25 T, respectively].

Formula (8) predicts no avoided crossings within the spectrum, and those as found in the exact diagonalization are due to the contribution of the excited radial states. In order to illustrate this fact further we performed a reference calculation restricted to the lowest-radial state. The reference calculation was performed in the following way: (1) We diagonalize the single-electron Hamiltonian *excluding the spin-orbit coupling*. (2) We form a basis of the obtained eigenfunctions selecting only those without zeroes outside the origin—thus excluding the excited radial states. (3) The basis obtained in

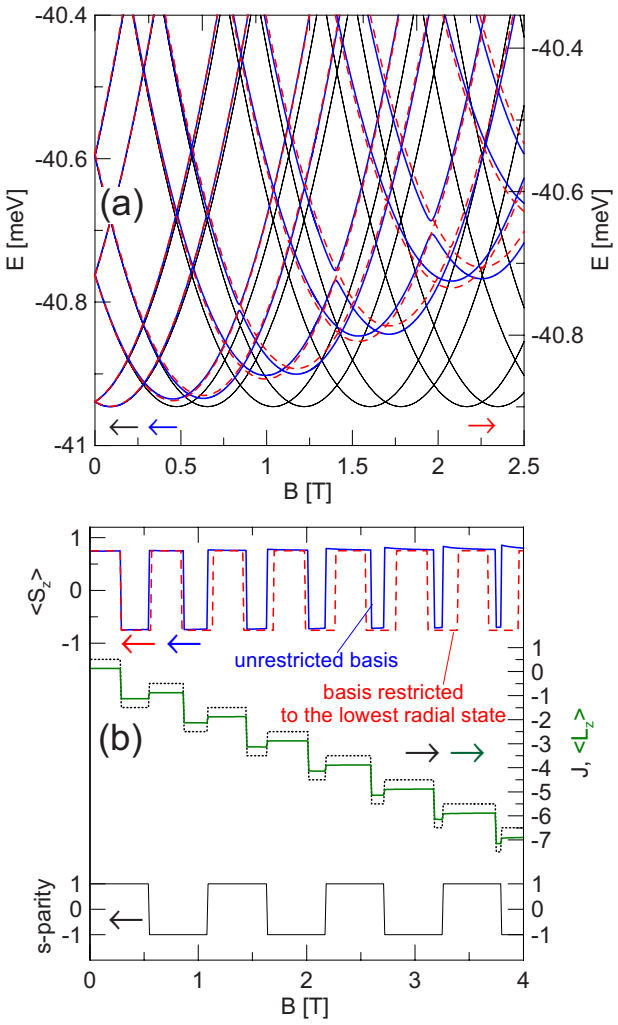

FIG. 2. (Color online) (a) Blue solid curves show the energy spectrum for a single type of the spin-orbit coupling [$\alpha=10.8$ meV nm, $\beta=0$ or equivalently $\alpha=0$, $\beta=10.8$ meV nm] for $g=0$ as obtained by the present approach. The black lines show the results given by the analytical formula Eq. (8) for a strictly one-dimensional quantum ring shifted down on the energy scale by −40.94 meV. The dashed red curves indicate the results obtained in the lowest-radial-state approximation (see text) referred to the right axis. (b) Solid blue and red dashed curves at the top of the plot show the value of the average spin as obtained for the two-dimensional quantum ring with the exact diagonalization approach and with the basis restricted to the lowest radial state, respectively. The black dotted line and the solid green line indicate the ground-state total and orbital angular momentum, respectively. The black solid line near the bottom of the plot shows the s parity of the ground state. Pure Rashba coupling was applied for this figure ($\alpha=10.8$ meV nm, $\beta=0$).

this way is used for diagonalization of the full Hamiltonian (1) including the spin-orbit coupling.

Results of the above procedure (lowest-radial-state approximation) were plotted in Fig. 2(a) with the dashed red curve with respect to the right axis. These results are shifted up on the energy scale by about 0.05 meV with respect to the exact result (mind the shift of the left and right energy scales), and the avoided crossings present in the exact spectrum are closed. In both the lowest-radial approximation and the exact calculation in the ground state one obtains only crossings of energy since the subsequent ground states correspond to different total angular momentum J quantum numbers [see Fig. 2(b)]. With each J transformation (ground-state level crossing) we observe a reorientation of the average spin [see the blue line in Fig. 2(b)]. We notice that the strict periodicity of the ground-state symmetry transformations as given by the one-dimensional formula (8) is perturbed at higher magnetic fields in the exact diagonalization spectrum. The Rashba interaction promotes ground states with spin-up orientation[51] and enlarges their ground-state stability range at the magnetic field scale at the expense of the spin-down oriented ground states. The magnetic fields for which the ground-state crossings are obtained in the lowest-radial-state approximation coincide with the ones produced by the analytical formula [see Fig. 2(a)] and the strict periodicity of the average spin oscillation is conserved [see the red dashed line in Fig. 2(b)].

For strictly one-dimensional rings the energy spectrum and the ground-state properties are ideally periodic with or without the spin-orbit coupling. For the two-dimensional ring considered here the ground-state angular-momentum transitions without the spin-orbit coupling appear nearly ideally periodically on the magnetic field scale (Fig. 1). The spin-orbit coupling destroys this periodicity [see the orbital angular momentum and the spin oscillation plotted with the blue line in Fig. 2(b)]. The periodicity is reproduced within the lowest-radial-state approximation [see the red dashed line for the average spin plotted in Fig. 2(b)] and not by the unrestricted basis.

We find that the first-excited state of the radial quantization contributes mostly to the minority-spin component of the ground-state wave function and we observe a shift of the maximum of the minority-spin density to a larger distance of the ring center with respect to the maximum of the majority-spin density (see Fig. 3). This shift is naturally overlooked by the lowest-radial-state approximation.

B. $\alpha=\beta$, $g=0$

Figure 4 shows the spectrum as obtained for $\alpha=\beta=10.8$ meV nm with the exact approach (blue solid curves) and with the basis restricted to the lowest-radial-state (red dotted curves) shifted down by 0.088 meV. For equal coupling constants both the exact and approximate energy levels are twofold degenerate. The restricted basis produces avoided crossings between the two lowest-energy levels and the rest of the spectrum (near $B=0$, 0.6, 1.2 T, etc.). The results obtained with the unrestricted basis do not contain any avoided crossings.

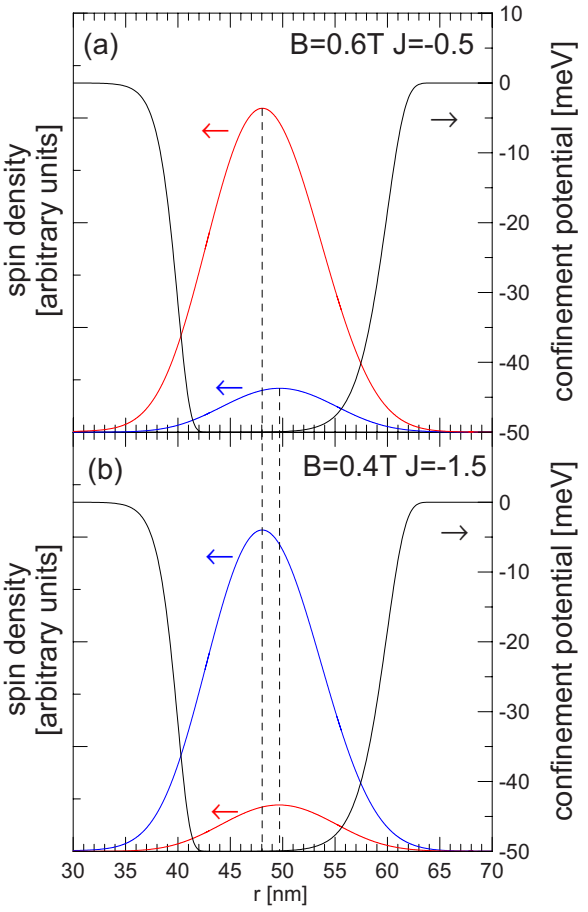

FIG. 3. (Color online) Spin-up (red curves) and spin-down densities (blue curves) as obtained in the ground-state for $B=0.6$ T (a) and $B=0.4$ T (b) for the pure Rashba coupling and $g=0$ (parameters of Fig. 2). The dashed vertical lines show the positions of the maxima of the majority and minority-spin distributions. The black solid lines show the confinement potential.

Figure 4(b) shows the ground-state charge density calculated as a function of the angle along the circumference of the ring for $r=50$ nm in the presence of the magnetic field of 0.75 T. We can see that the restricted basis produces deformation of the charge density, with no counterpart in the exact result. In Fig. 5 we additionally plotted the charge and spin densities for the odd s-parity ground state[49] at $B=0.75$ T, as obtained in the lowest-radial-state approximation [Fig. 5(a)] and by the exact diagonalization [Fig. 5(b)]. Although the spin densities in the approximate and exact results similarly deviate from the circular symmetry, in the exact result they are distributed in a way that their sum is exactly circularly symmetric, which is not reproduced in the restricted basis [Fig. 5(a)].

We found that the deviation of the charge density from circular symmetry that occurs due to the spin-orbit coupling has an elliptic character, i.e., the charge density is symmetric with respect to both the diagonal line $x=y$ (crystal direction [110]) and the antidiagonal line $y=-x$ (crystal direction $[1\bar{1}0]$). In consequence the charge density acquires extremal values on the crossing of the average ring radius and the

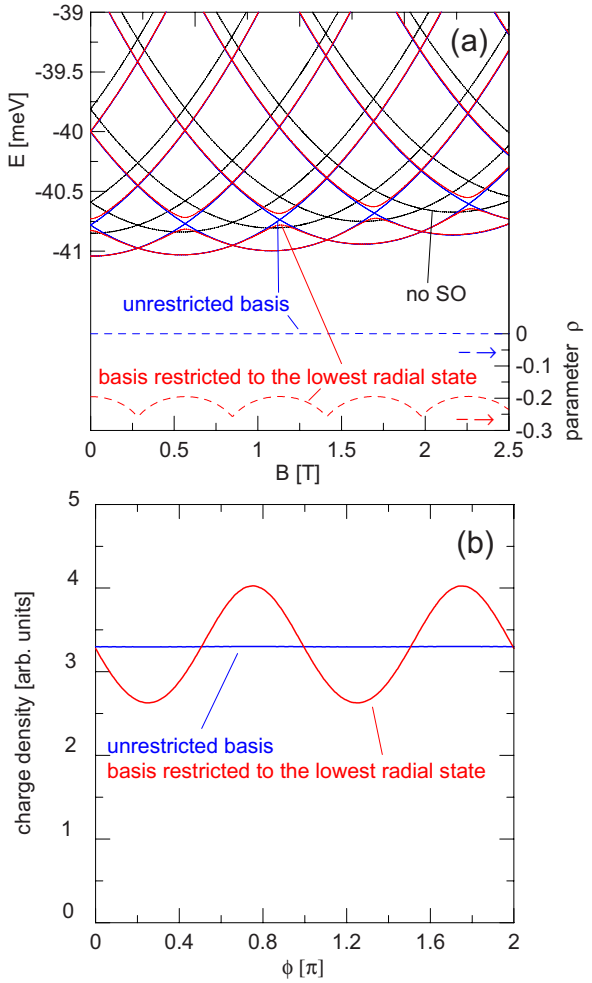

FIG. 4. (Color online) (a) Blue solid curves show the spectrum for $\alpha=\beta=10.8$ meV nm and $g=0$ as obtained with the unrestricted basis. Red dotted curves indicate the results of the lowest-radial-state approximation shifted down on the energy scale by 0.088 meV. The black dotted curves show the results for the spin-orbit coupling excluded. The dashed lines show the parameter ρ characterizing deviation of the charge density from the circular symmetry [Eq. (9)], as obtained by the exact diagonalization (blue line) and with the lowest-radial-state approximation (red line). (b) Charge density obtained for $B=0.75$ T plotted along the center of the ring $r=50$ nm as obtained by the exact diagonalization (blue curve) and with the basis restricted to the lowest radial state (red line) for the ground state of odd s parity.

symmetry axes. Therefore, in order to quantify the elliptic deformation of the charge density we use a parameter

$$\rho = \frac{|\Psi(\pi/4)|^2 - \langle|\Psi|^2\rangle}{\langle|\Psi|^2\rangle}, \tag{9}$$

where $\langle|\Psi|^2\rangle$ is the average electron density calculated over the angle along the circumference of the ring at a distance of 50 nm of its center, and $|\Psi(\pi/4)|^2$ is the value obtained for the angle $\pi/4$, i.e., in point of Cartesian coordinates $x=y=35.33$ nm [see Fig. 5]. The ρ values as obtained with the restricted and unrestricted bases are plotted at the lower part of Fig. 4(a). In the lowest-radial-state approximation the parameter is negative (one obtains density minima at [110] direction), and the strongest deformation is obtained near the ground-state-symmetry transformations—at odd multiples of half of the flux quantum. In the discussed case of equal coupling constants and $g=0$ the unrestricted basis produces ideally circular results and parameter ρ is found equal to zero.

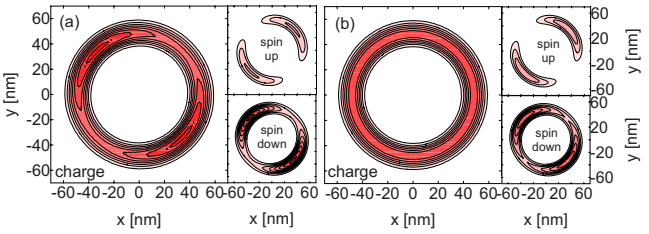

FIG. 5. (Color online) Charge and spin densities as obtained for $g=0$, $\alpha=\beta=10.8$ meV nm and $B=0.75$ T in the basis restricted to the lowest-radial-state (a) and in the unrestricted basis (b) for the ground state of odd s parity (for the ground state of even s parity the spin-up and spin-down densities are inverted).

The effects found in the basis restricted to the lowest radial state, i.e., the opening of the avoided crossings in the energy spectrum [Fig. 4(a)] and the charge-density deformation [Figs. 4(b) and 5(a)], including the orientation of the charge-density maxima on the antidiagonal of the ring ($y=-x$ line) agree with the results of the one-dimensional model presented in Fig. 7(a,b) of Ref. 34 obtained for $\alpha=\beta$ and $g=0$. However, none of these results is reproduced by the unrestricted basis [see Figs. 4(a) and 5(b)]. These effects turn out to be artifacts of the basis restricted to the lowest radial state. In fact, both the appearance of the avoided crossings in the energy spectrum and the charge-density deformation are excluded by the intrinsic symmetry of the Hamiltonian (1) present for $\alpha=\beta$ and $g=0$ as pointed out in Ref. 2. For $\alpha=\beta$ and $g=0$ (i) the Hamiltonian commutes with $\sigma_x-\sigma_y$ operator.[2,50] (ii) The spin-orbit coupling shifts down the entire spectrum by a constant value $2\alpha^2 m^*/\hbar^2$. (iii) The charge density for each of the Hamiltonian eigenstates is not affected by the spin-orbit coupling.

The results presented above for the nonrestricted basis exactly reproduce all the above features including the constant downshift of the spectrum [for $\alpha=10.9$ meV nm equal to 0.19 meV—the spectrum without spin-orbit coupling is plotted with the black dotted lines in Fig. 4(a)].

For $\alpha=\beta$ and $g=0$ the circular symmetry of the charge density results from the intrinsic symmetry of the Hamiltonian and its deformation is excluded independent of the thickness of the ring. In consequence there does not exist a ring thickness w small enough for which the exact results could reproduce the deformation of the charge density produced by the lowest-radial-state approximation. In other words, the limitation of the basis to the lowest radial state does not become a good approximation even in the limit of small w, although the energy spacing between the lowest-energy and first-excited state diverge as $1/w^2$, which seems quite counterintuitive. A related fact—a nonvanishing contribution of the excited Landau levels in the infinite magnetic field limit of spin-orbit coupled quantum dots for $g=0$—was recently indicated in Ref. 51.

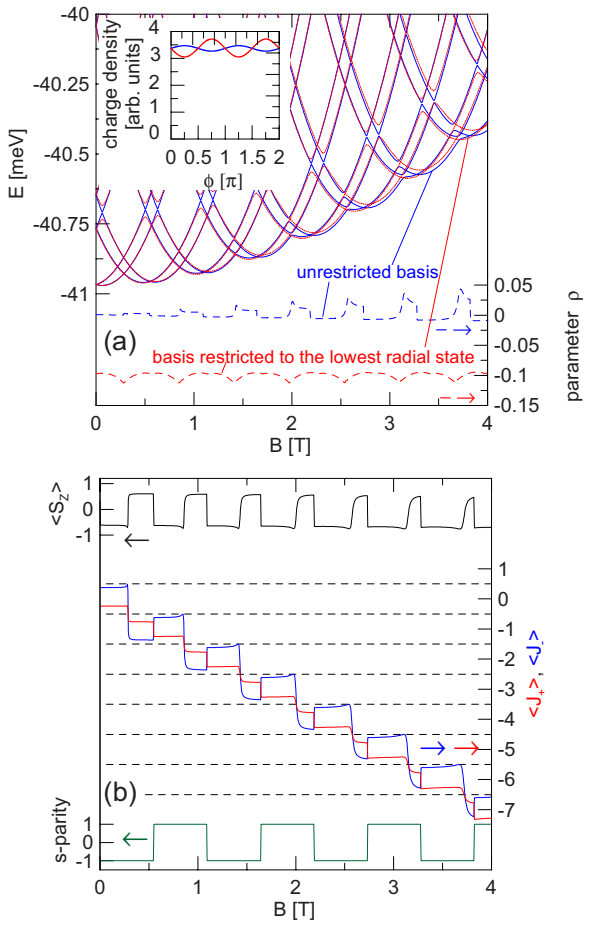

FIG. 6. (Color online) (a) The blue solid and the red dotted curves show the spectrum as calculated for $\alpha=\beta/2=5.4$ meV nm with the unrestricted basis and in the lowest-radial-state approximation, respectively. The dashed curves indicate the value of the ρ parameter as calculated by the exact (blue) and restricted (red) bases. The inset shows the ground-state charge density for $B=3.77$ T along the circumference of the ring as obtained by the basis restricted to the lowest radial state (red curve) and for unrestricted basis (blue curve). (b) The black line at the top of the plot show the average value of the z component of the spin, the blue and red lines the average values of the J_- and J_+ total angular-momentum operators, and the green line near the bottom of the plot the ground-state s-parity obtained in the exact calculation.

C. $\alpha \neq \beta$, $g=0$

When both coupling types are present but nonequal, there does not exist a direction in which the spin component would commute with the Hamiltonian, and in general energy levels in the external magnetic field are nondegenerate. The spectrum for $\alpha=5.4$ meV nm and $\beta=10.8$ meV nm is plotted in Fig. 6—the blue curves show the exact results and the dotted red ones indicate the results obtained with the basis restricted to the lowest radial state shifted down by 0.057 meV. In the ground state we observe regular s-parity transformations [Fig. 6(b)] like in the case of pure Rashba coupling of Fig. 2. However, the total angular momentum is no longer quantized in the Hamiltonian eigenstates [Fig. 6(b)]. Since the considered case corresponds to the dominant Dresselhaus coupling the J_- average values are closer to the stepwise dependence observed for a single coupling type present of Fig. 2 than J_+. Also, since the Dresselhaus coupling dominates—the stability of spin-down ground states is observed at high field, like in the case of parabolic quantum dots.[51]

Let us now focus our attention on the first ground-state transformation observed near 0.25 T. For the pure and weak Dresselhaus coupling[53] one obtains here a crossing of spin-down $l=0$ eigenstate and spin-up $l=-1$ energy levels. Both these levels correspond to odd s-parity symmetry; however there is no avoided crossing between them since they correspond to different quantum numbers $J_-=1/2$ and $J_-=-3/2$ (opposite spin orientation) before and after the crossing, respectively. For nonzero Rashba coupling accompanying the dominant Dresselhaus coupling that is considered in Fig. 6 the drop of J_- value from about $1/2$ to about $-3/2$ near 0.25 T is continuous since the two energy levels enter into a narrow avoided crossing. The actual crossings in the spectrum are obtained only when the ground-state s-parity changes [see Fig. 6(b)] and they are accompanied by jumps in the average value of J_-. For instance near $B=2.75$ T there is a ground-state crossing and for $B=3.1$ T—an avoided crossing occurs [see Fig. 6(a)]. The ground-state energy-level anticrossings are overlooked by the lowest-radial-state approximation [see the red dotted lines in Fig. 6(a)].

The deformation of the ground-state charge density as obtained by the exact diagonalization occurs only near the ground-state avoided crossings and becomes more pronounced at higher field—see the deformation parameter ρ plotted in Fig. 6(a) with the blue dashed line. The exact value of the deformation parameter is a few times smaller than the one obtained in the lowest-radial-state approximation. Moreover, a detectable elliptical deformation of the charge density in the exact result is only obtained for finite magnetic field, while in the lowest-radial-state approximation the parameter ρ takes a nonzero value already at $B=0$. Parameter ρ as obtained by the exact diagonalization occasionally acquires positive sign, opposite to the one obtained in the lowest-radial-state approximation. Then, the maxima of the charge density as calculated by the exact diagonalization appear on the diagonal line $x=y$, while in the lowest-radial-state approximation charge-density minima are found on the antidiagonal $x=-y$. The exact and approximate charge densities are plotted in the inset to Fig. 6 for $B=3.77$ T, when a maximal deformation is obtained in the exact calculation.

For a ring of smaller width the results of the lowest-radial-state approximation should be closer to the exact ones. In order to verify this expectation we considered a ring with the inner radius $R_i=55$ nm and the outer one $R_o=60$ nm with potential depth $V_0=200$ meV. The ground-state avoided crossing becomes too thin to be observed (see Fig. 7). The spectrum in the lowest-radial-state approximation becomes nearly identical to the exact one with the exception of a constant variational overestimate of about 0.067 meV and an artificial energy gap opened near −281.8 meV. The ground-state spin oscillation as calculated in the unrestricted basis retains its periodicity in the considered magnetic field range [Fig. 7(b)]. A pronounced difference is still found in the confined charge density. The deformation of the exact charge density disappears with narrowing of the ground-state

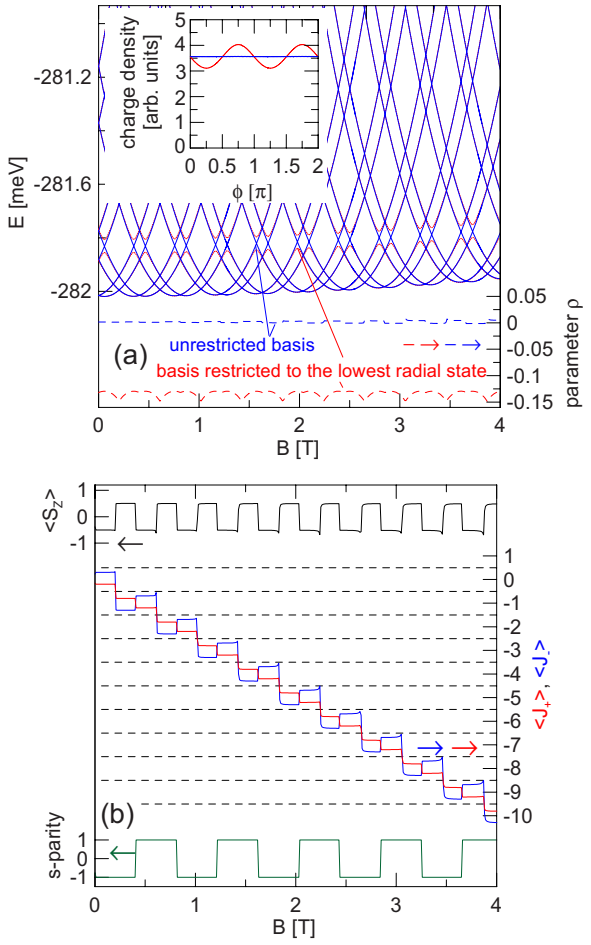

FIG. 7. (Color online) Same as Fig. 6 but for a ring of four times smaller width: R_i=55 nm and R_o=60 nm. The energy spectrum obtained by the restricted basis in (a) was shifted down by 0.067 meV.

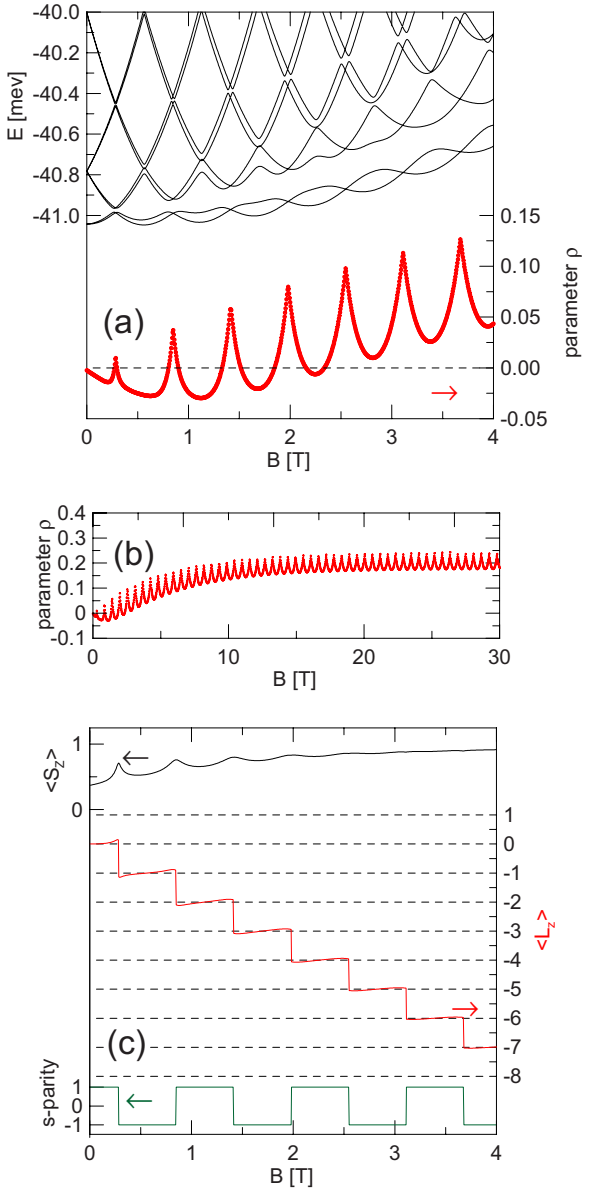

FIG. 8. (Color online) (a) Black curves show the energy spectrum as calculated by the exact diagonalization for $\alpha=\beta$ =10.8 meV nm and $g=-2.15$. The red symbols show the deformation parameter ρ, which in wider B range is presented also in panel (b). (c) The black curve at the top of the plot shows the ground-state average value of the spin component, the red curve presents the average orbital angular momentum and the plot at the bottom of the plot indicates the s parity.

energy-level crossings and becomes too weak to be observed (inset to Fig. 7), while the deformation obtained in the lowest-radial-state approximation not only remains, but is increased by a factor of 50% with respect to the case of Fig. 6 [see the deformation parameters in Figs. 6(a) and 7(a)]. In the context of the charge-density deformation the results of the lowest-radial-state approximation do not really become closer to the results of the exact diagonalization in the limit of small ring width.

D. $g=-2.15$

The spin Zeeman effect for perpendicular magnetic field introduces σ_z operator into the Hamiltonian. With the Zeeman effect and the spin-orbit coupling present there does not exist any spin component whose operator would commute with the Hamiltonian even for $\alpha=\beta$, which lifts the hidden symmetry of the Hamiltonian[2] discussed above. The spectrum for $g=-2.15$ and $\alpha=\beta=10.8$ meV nm is plotted in Fig. 8(a). We can see that two lowest-energy levels separate from the rest of the spectrum and the ground state undergoes s-parity oscillations [see Fig. 8(c)] in the external magnetic field. The Zeeman effect promotes the spin-up orientation [Fig. 8(c)] at high field. The charge density distinctly deviates from the circular symmetry [cf. deformation parameter plotted in Fig. 8(a)]. The deformation parameter takes on maximal values at the ground-state s-parity transformations and it stays positive above 2.5 T [see Fig. 8(b)], i.e., with charge-density maxima localized on the diagonal of the ring—see Fig. 9 for B=2 T. The maximal value of ρ parameter at the ground-state s-parity transformations implies that the deviation from the circular symmetry is stronger in the excited state than in the ground-state—see Fig. 9.

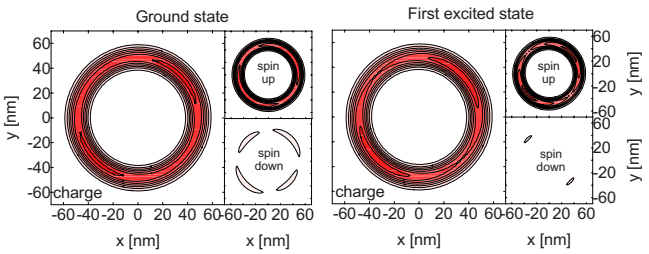

FIG. 9. (Color online) Charge and spin densities for the parameters considered in Fig. 8 at $B=2$ T.

For $\alpha=\beta=0$ the electron density remains circular, no avoided crossings are observed in the spectrum of definite orbital angular momenta [see Fig. 10(a)], and a complete ground-state spin polarization is observed for any nonzero B.

The energy spectrum, the ground-state spin, orbital angular momentum, and s parity are presented in Fig. 11 for nonequal and nonzero coupling constants, namely, for $\alpha=\beta/2=5.4$ meV nm. The results qualitatively agree with the ones

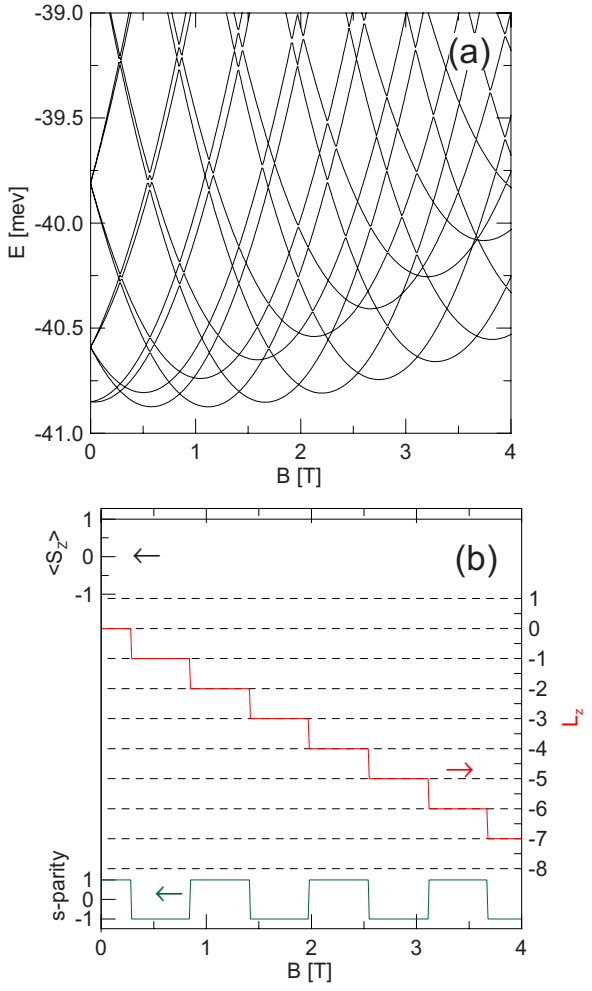

FIG. 10. (Color online) (a) Black curves show the energy spectrum as calculated by the exact diagonalization for $\alpha=\beta=0$ and $g=-2.15$. (b) The black curve at the top of the plot shows the ground-state value of the spin component, the red curve presents the orbital angular momentum and the plot at the bottom of the plot indicates the s-parity.

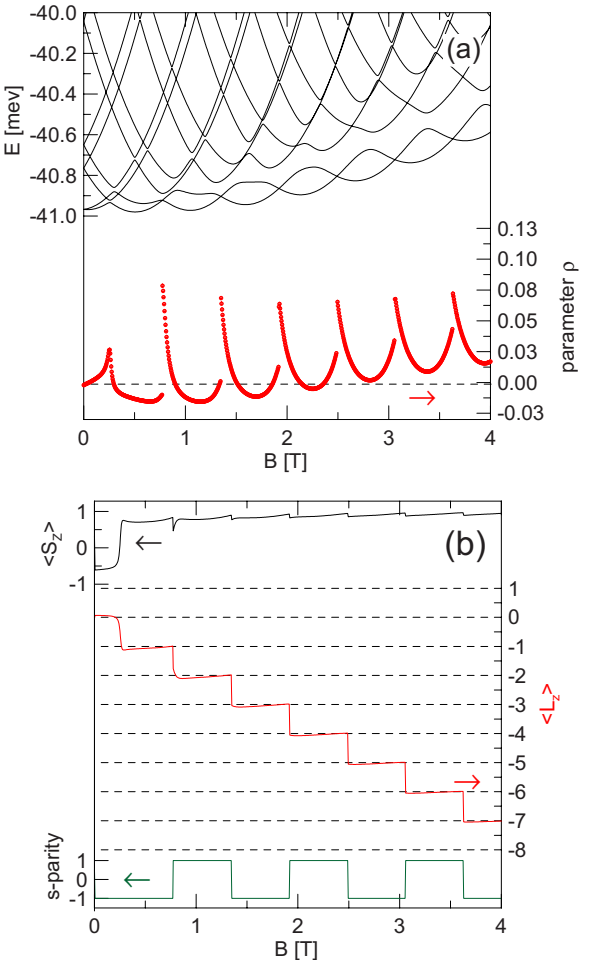

FIG. 11. (Color online) Same as Fig. 8 but for $\alpha=\beta/2=5.4$ meV nm, $g=-2.15$.

obtained for $\alpha=\beta$ in Fig. 8. In particular, an energy gap between two lowest-energy states of opposite parities and the rest of the spectrum is opened and maximal deformation of the electron density is found at the ground-state s-parity transformations. However, the ρ parameter is no longer continuous at the symmetry transformations [cf. the case of $\alpha=\beta$ of Fig. 8(a)]

For one of the coupling constants equal to zero either J_+ or J_- operator commutes with Hamiltonian, hence no deformation of the electron density is found, and the energy spectrum (Fig. 12) does not contain any energy gap between two lowest-energy levels and the rest of the spectrum—in contrast to Figs. 8 and 11.

E. Two confined electrons

Figure 13(a) shows the two-electron spectrum for $g=0$ in the absence of the spin-orbit coupling. The magnetic period of the ground-state transitions is halved[22] with respect to the single-electron case (compare Figs. 1 and 13). Figure 13(b) presents the spectrum for the highly symmetric spin-orbit coupling of $\alpha=\beta=10.8$ meV nm. In Fig. 13 the two-electron

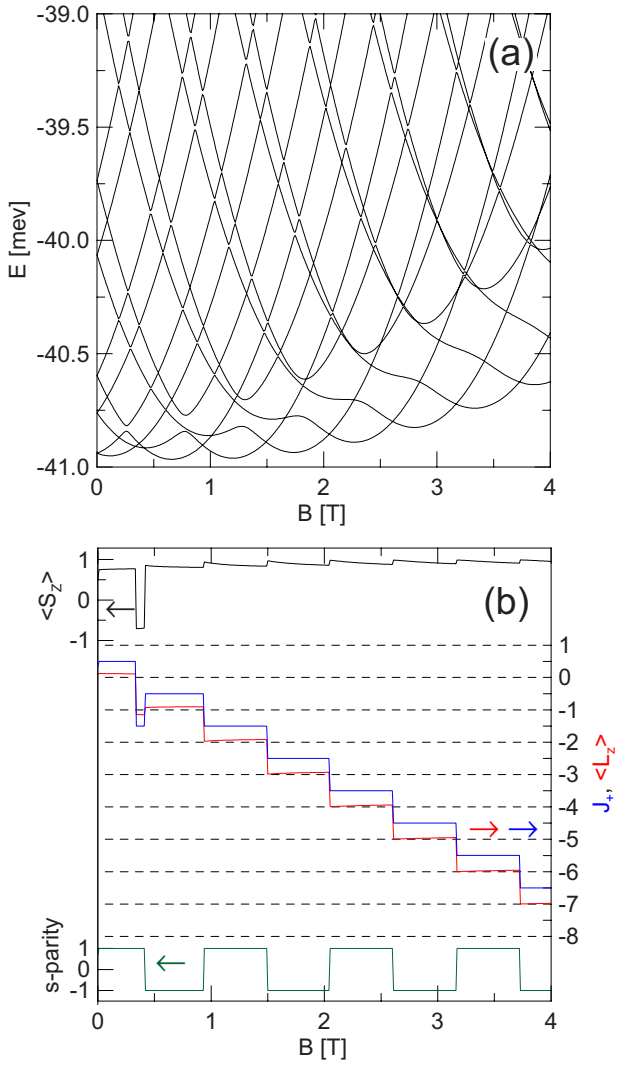

FIG. 12. (Color online) Same as Fig. 11 but for $\alpha = 10.8$ meV nm, $\beta = 0$ and $g = -2.15$.

spectrum is only shifted down by the spin-orbit coupling by the energy of 0.38 meV, which is twice the value of the shift $2(\alpha^2 m^*/\hbar^2)$ for a single electron (see Sec. III B). No other difference is found between the spectra presented in Figs. 13(a) and 13(b). The invariance of the spectrum although due to the symmetry of the Hamiltonian, in the exact diagonalization calculation is only reproduced by a fully convergent two-electron basis, which illustrates the strength of the present numerical approach.

In the absence of the spin-orbit coupling, in two-electron quantum rings as well as in quantum dots the ground-state spin triplets (singlets) correspond to odd (even) orbital angular momenta, and the ground-state total spin quantum number oscillates between 0 and 1 in the external magnetic field. When the Zeeman effect is included the spin oscillations vanish at higher field and the state with spins polarized parallel ($g < 0$) to the magnetic field vector is established as the ground state. This spin-up polarized ground state of the odd orbital angular momentum corresponds to the odd s-parity symmetry. The even and the odd s-parity energy levels for $g = -2.15$ are plotted in Fig. 14(a) for $\alpha = \beta = 0$ with the red and blue curves, respectively. Note that the Zeeman effect lifts the fractional[22] Aharonov-Bohm oscillation for two confined electrons and leaves an integral period shifted by half of the flux quantum with respect to the single-electron oscillation. For $\alpha = \beta = 10.8$ meV nm [see Fig. 14(b)] the ground-state crossings—which for $\alpha = \beta = 0$ are due to the orbital angular-momentum transitions—are replaced by avoided crossings between the odd s-parity energy levels. Opening of avoided crossings is more evident for a case of a weaker spin-orbit coupling $\alpha = \beta = 5.4$ meV nm presented in Fig. 14(c).

In Fig. 15 the two-electron ground-state charge and spin densities for $B = 4$ T are presented for $\alpha = \beta = 10.8$ meV nm. The left column of plots [Figs. 15(a) and 15(c)] corresponds to $g = 0$, the right column to $g = -2.15$ [Figs. 15(b) and 15(d)]. In the upper row of plots [Figs. 15(a) and 15(b)] the electron-electron interaction is neglected and it is included in the lower row of plots [Figs. 15(c) and 15(d)]. For $g = 0$ both the

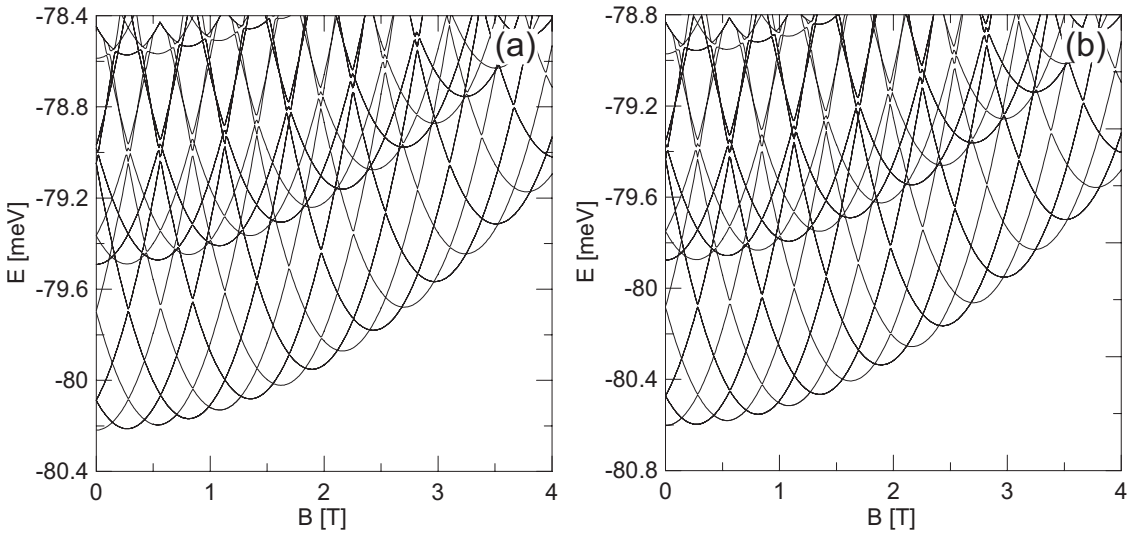

FIG. 13. Two-electron spectrum for $g = 0$ in the absence of the spin-orbit coupling (a), and for $\alpha = \beta = 10.8$ meV nm (b).

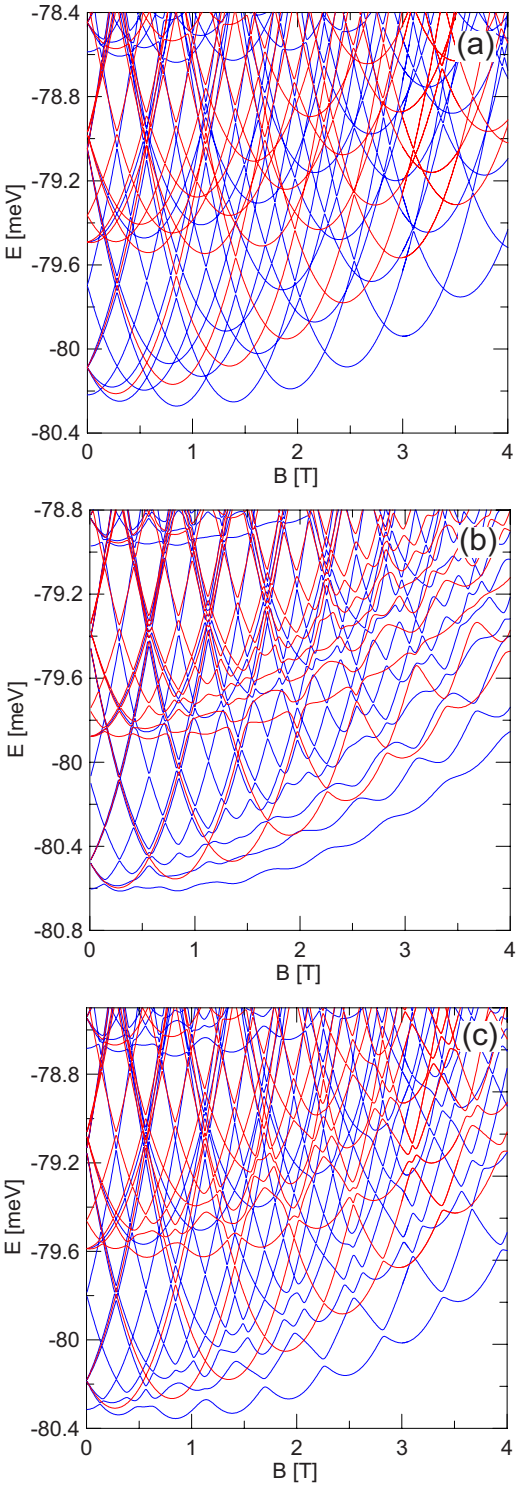

FIG. 14. (Color online) Two-electron energy spectrum for $g=-2.15$ and equal coupling constants $\alpha=\beta$. Blue (red) curves show the energy levels of odd (even) s-parity. Plots (a), (b) and (c) correspond to $\alpha=0$, $\alpha=10.8$ meV nm, and $\alpha=5.4$ meV nm, respectively.

spin and charge density remain circularly symmetric. In the case of single-electron s-parity eigenstates the spin-up and spin-down densities were noncircular although their sum reproduced the circular symmetry [Fig. 5(b)]. For a single electron ($\alpha=\beta$, $g=0$) the ground state is twofold degenerate with interchanged spin densities for the odd and even s-parity ground states. For two confined electrons one of them occupies the odd s-parity state and the other the even s-parity state. The two-electron ground state is therefore nondegenerate and the spin densities sum up to a circularly symmetric distribution. For nonzero g, and $\alpha=\beta$ the two-electron ground-state density—even without the electron-electron interaction—is more strongly deformed than the single-electron ground-state density. This is because in the first-excited single-electron state—which is also occupied in the two-electron ground state—the elliptic deformation is stronger than in the single-electron ground state. Moreover the single-electron ground state and the first-excited state possess charge-density maxima at the same $y=x$ line [see the maximal value of the deformation parameter at the ground-state symmetry transformations presented in Fig. 8(a)]. The electron-electron interaction makes the elliptic deformation of the charge density even stronger [cf. Figs. 15(b) and 15(d)].

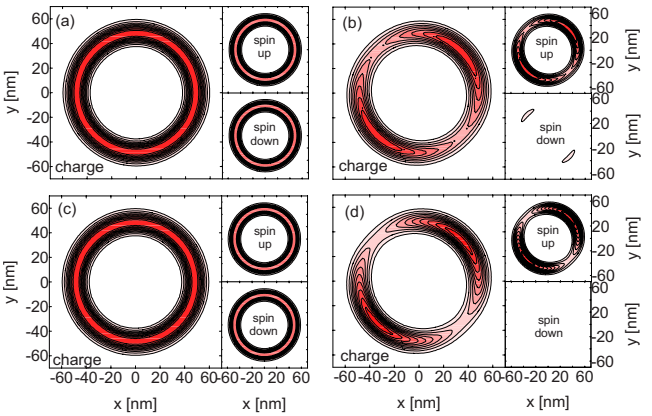

FIG. 15. (Color online) Two-electron charge and spin ground-state densities for $B=4$ T for $\alpha=\beta=10.8$ meV nm. $g=0$ is assumed in (a) and (c), and $g=-2.15$ in (b) and (d). Electron-electron interaction is neglected in (a), (b) and accounted for in (c), (d).

The elliptic deformation parameter ρ for two electrons and $g=-2.15$ is plotted in Fig. 16. The blue curves correspond to $\alpha=\beta=10.8$ meV nm with (solid curve) and without (dashed curve) electron-electron interaction. The electron-electron interaction strongly enhances the elliptic deformation of the charge density particularly at odd multiples of half quantum (0.565 T), which correspond to crossings of triplet states in the absence of the spin-orbit coupling [see Fig. 14(a)]. The black line in Fig. 16 shows the result obtained for $\alpha=\beta/2=5.4$ meV nm (electron-electron interaction included). Dependence of the parameter ρ on the magnetic field is very similar to the one found for equal coupling constants.

F. Magnetization and single-electron charging properties

Theoretical analysis of the spin-orbit coupling effects presented above required discussion of the special case of $g=0$. For the experimentally relevant quantities we limit the

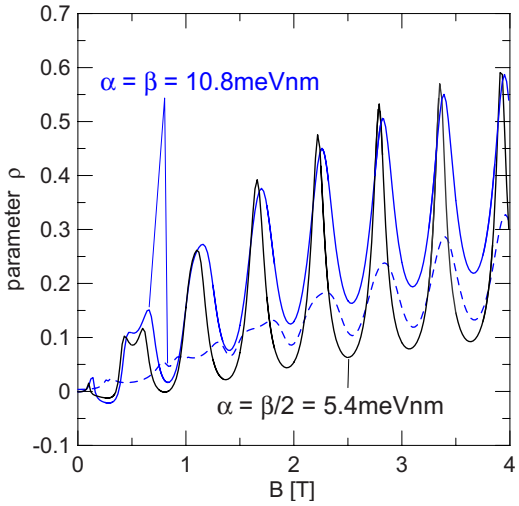

FIG. 16. (Color online) Parameter ρ quantifying the deviation of the electron density from the circular symmetry as obtained for two electrons for $\alpha=\beta=10.8$ meV nm and $g=-2.15$ with (blue solid line) and without electron-electron interaction (blue dashed line). The black solid line corresponds to $\alpha=\beta/2=5.4$ meV nm (electron-electron interaction included).

discussion to the case of negative Landé factor specific to InGaAs structures.

Figures 17 and 18 show the magnetization ($M=-\frac{dE}{dB}$) produced by a single and two electrons. Figure 17 presents the case of pure Rashba and pure Dresselhaus coupling as compared to the results obtained without the spin-orbit interaction. For $B>2$ T the magnetization for both pure Rashba and pure Dresselhaus interactions acquire the same periodicity as in the absence of spin-orbit coupling only the magnetic fields for which the discontinuities appear (due to the ground-state total angular-momentum transitions) are slightly shifted to lower (for Dresselhaus coupling) or higher (for Rashba coupling) values.

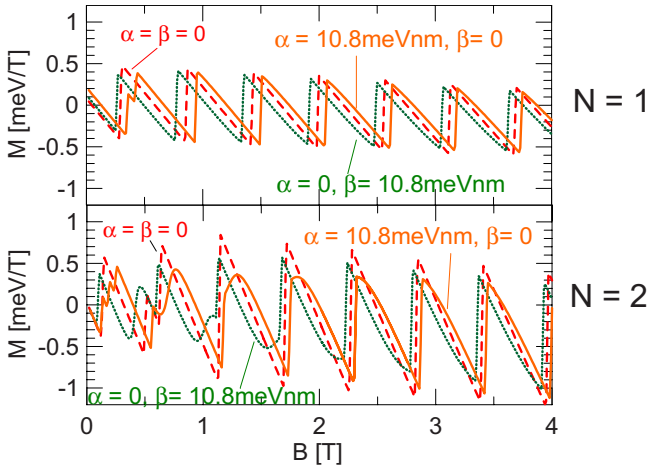

FIG. 17. (Color online) Magnetization for a single (upper plot) or two confined electrons (lower plot) without the spin-orbit coupling and for a single type of the spin-orbit coupling present. $g=-2.15$ is assumed for the Landé factor.

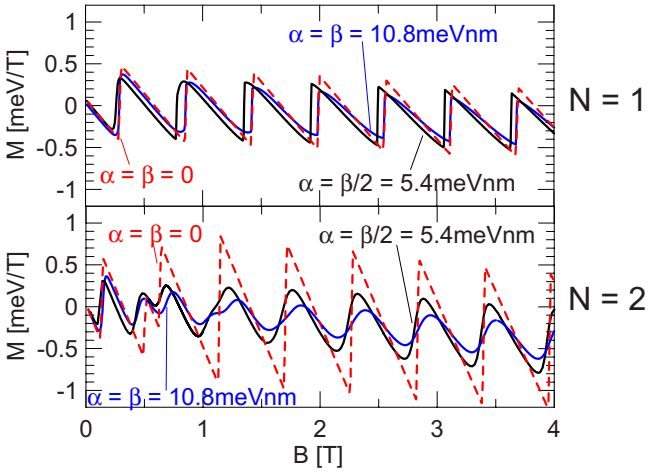

FIG. 18. (Color online) Magnetization for a single (upper plot) or two confined electrons (lower plot) without the spin-orbit coupling and for both types of spin-orbit coupling present. $g=-2.15$ is assumed for the Landé factor.

For both coupling constants nonzero the magnetization discontinuities result from the s-parity transformations. For a single electron the magnetization dependence on the magnetic field (see upper panel of Fig. 18) is similar to the one presented in Fig. 17 for a single type of spin-orbit coupling present. A qualitatively different result between the case of a single and both types of spin-orbit coupling present is obtained for two confined electrons (cf. lower panels of Figs. 17 and 18). For both coupling constants nonzero the ground state already for relatively weak magnetic field becomes permanently s-odd and the ground-state crossings due to the s-parity transformations disappear of the ground-state energy level [see Figs. 14(b) and 14(c)]. In consequence the two-electron magnetization becomes a continuous function of the magnetic field, in contrast to both the case of $\alpha=\beta=0$ and a single type of the spin-orbit coupling present. We also observe that the amplitude of the magnetization oscillations is reduced when both spin-orbit coupling types are present (Fig. 18). This reduction results from hindered circulation of the persistent currents around the ring due to appearance of the charge-density minima. The magnetization reduction is slight for a single electron and more pronounced for two electrons, in accordance with the relative strength of the elliptic deformation for one and two confined electrons.

In the single-electron charging experiments[43] the quantum rings embedded in a charge tunable structure are occupied by subsequent electrons when the chemical potentials of N-electron system is aligned with the Fermi energy of the electron reservoir. The chemical potential is defined as $\mu_N=E_N-E_{N-1}$, where E_N stands for the ground-state energy of N confined electrons. The chemical potentials for one- and two-electron systems are plotted in Fig. 19 for a single type of spin-orbit coupling and in Fig. 20 for nonzero values of both α and β coupling constants. The single-electron chemical potential depends on the magnetic field in a qualitatively the same manner in all the cases considered in Figs. 19 and 20. A qualitative difference is obtained for two electrons. The chemical potential for $N=2$ without the spin-orbit coupling

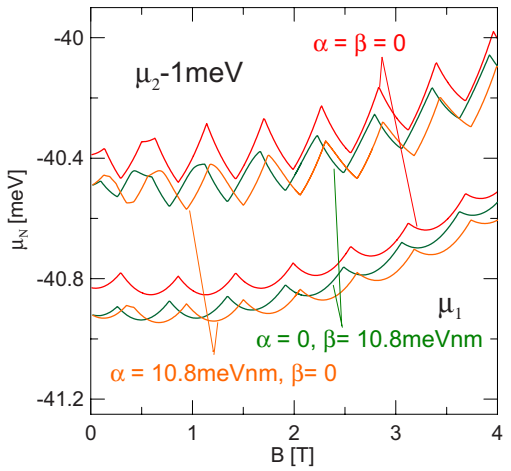

FIG. 19. (Color online) Chemical potentials for one (three lower curves) and two (three upper curves) confined electrons without the spin-orbit coupling and for a single type of spin-orbit coupling present ($g=-2.15$). The chemical potential for two electrons is shifted down by 1 meV.

has cusps (discontinuous derivatives) whenever the ground-state symmetry transformations occur for one or two electrons. The ground-state symmetry transformations for $N=1$ result in V-shaped cusps and the transformations for $N=2$ in Λ-shaped cusps. In Fig. 20 we notice that when both spin-orbit coupling types are present the Λ-shaped cusps in μ_2 are replaced by smooth maxima, which is related to the avoided crossings between s-odd-parity energy levels that are opened in the low part of the energy spectrum [Figs. 14(b) and 14(c)].

Both the magnetization and the chemical potential as presented in Figs. 17–20 indicate that the case of two electrons for both spin-orbit coupling types present differs qualitatively from the case when a single or no type of spin-orbit coupling is present. Above we demonstrated that for

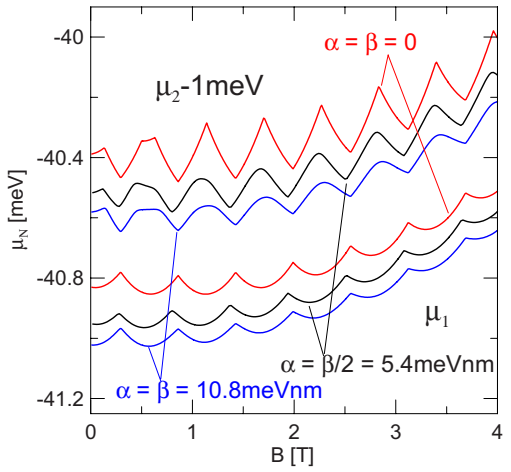

FIG. 20. (Color online) Chemical potentials for one (three lower curves) and two (three upper curves) confined electrons without the spin-orbit coupling and for both types of spin-orbit coupling present ($g=-2.15$). The chemical potential for two electrons is shifted down by 1 meV.

$g=-2.15$ when both coupling constants are nonzero the ground-state electron density is subject to an elliptical deformation. For a single type of spin-orbit coupling present as well as in the absence of the spin-orbit coupling no elliptical deformation is found. Magnetization and chemical potential as obtained for two electrons and both spin-orbit coupling types present have qualitatively the same dependence on the magnetic field as the one found recently for a circular quantum ring with two symmetrically placed repulsive defects[52] in the absence of the spin-orbit coupling. Figure 15(c) of Ref. 52 shows that the Λ-shaped cusps disappear of the two-electron chemical potential, and Fig. 16(c) of the same work demonstrates that the two-electron magnetization becomes a continuous function of the magnetic field when the ground state acquires the odd spatial parity for stronger magnetic field. Reference 52 also demonstrates that for a single electron confined in a circular ring with two symmetrically placed defects, both the chemical potential and the magnetization remain qualitatively the same as for the clean—circular quantum ring—due to the spatial parity ground-state transformations replacing the angular-momentum transitions for the clean ring. Therefore, at least for one and two electrons, the elliptical deformation of the charge density, which is found in a circular ring when both spin-orbit coupling types are present, results in the same consequences for both the charging and the magnetic properties of the ring as an elliptical perturbation of the circular quantum ring potential in the absence of the spin-orbit coupling.

IV. SUMMARY AND CONCLUSIONS

We have performed a systematic exact diagonalization study of spin-orbit coupling effects for one and two electrons confined in a circular quantum ring of finite width. We discussed validity of one-dimensional models assuming that the radial functions of confined carriers can be identified with the lowest-energy radial state as obtained without the spin-orbit coupling. For a single type of spin-orbit coupling present the lowest-radial-state approximation overlooks rather secondary effects: (i) some avoided crossings that appear in the excited part of the spectrum, (ii) nonideal periodicity of the ground-state oscillation of the average spin obtained for $g=0$, and (iii) relative radial shifts of the majority and minority-spin densities. The performance of the lowest-radial-state approximation is worse when both Rashba and Dresselhaus coupling types are present. In that case the lowest-radial-state approximation produces charge densities which differ qualitatively from the exact ones. In particular for equal coupling constants in the absence of the Zeeman effect the basis restricted to the lowest radial state produces charge densities with artifactally broken circular symmetry, which at least for some applications excludes the usage of the one-dimensional models when Dresselhaus and Rashba spin-orbit interactions are simultaneously present. We have demonstrated that the charge density as obtained by the exact diagonalization deviates from the circular symmetry only when the Zeeman effect is present or when the coupling constants are nonequal. The elliptical deformation of the single-electron density that is found by the exact diagonal-

ization is generally weaker than in the lowest-radial-state approximation and with a different orientation of the density maxima. Moreover, the actual elliptic deformation of the charge density is only obtained for finite magnetic fields, while in the lowest-radial-state approximation the deformation is already found at $B=0$. We have considered signatures of the charge-density deformation on experimentally relevant quantities. We have found that the elliptical deformation of the charge density that appears due to the interplay of the spin-orbit coupling and the Zeeman effect has similar consequences for the magnetization and charging properties of the ring as an elliptical deformation of the circular quantum ring confinement potential in the absence of the spin-orbit coupling.

ACKNOWLEDGMENTS

This work was supported by the "Krakow Interdisciplinary Ph.D.-Project in Nanoscience and Advanced Nanostructures" operated within the Foundation for Polish Science MPD Programme, co-financed by the EU European Regional Development Fund. Calculations were performed in ACK–CYFRONET–AGH on the RackServer Zeus.

[1] S. Datta and B. Das, Appl. Phys. Lett. **56**, 665 (1990).
[2] J. Schliemann, J. C. Egues, and D. Loss, Phys. Rev. Lett. **90**, 146801 (2003).
[3] K. C. Nowack, F. H. L. Koppens, Yu. V. Nazarov, and L. M. K. Vandersypen, Science **318**, 1430 (2007).
[4] S. Bednarek and B. Szafran, Phys. Rev. Lett. **101**, 216805 (2008).
[5] P. Földi, B. Molnar, M. G. Benedict, and F. M. Peeters, Phys. Rev. B **71**, 033309 (2005); P. Földi, O. Kalman, M. G. Benedict, and F. M. Peeters, Nano Lett. **8**, 2556 (2008).
[6] S. Bellucci and P. Onorato, Phys. Rev. B **77**, 165305 (2008).
[7] E. Tsitsishvili, G. S. Lozano, and A. O. Gogolin, Phys. Rev. B **70**, 115316 (2004).
[8] P. Pietiläinen and T. Chakraborty, Phys. Rev. B **73**, 155315 (2006).
[9] M. S. Kushwaha, J. Appl. Phys. **104**, 083714 (2008).
[10] W. H. Kuan, C. S. Tang, and W. Xu, J. Appl. Phys. **95**, 6368 (2004).
[11] T. Chakraborty and P. Pietiläinen, Phys. Rev. Lett. **95**, 136603 (2005).
[12] M. Valin-Rodriguez, A. Puente, and L. Serra, Phys. Rev. B **69**, 153308 (2004).
[13] P. Lucignano, B. Jouault, A. Tagliacozzo, and B. L. Altshuler, Phys. Rev. B **71**, 121310(R) (2005).
[14] C. F. Destefani, S. E. Ulloa, and G. E. Marques, Phys. Rev. B **70**, 205315 (2004).
[15] D. V. Bulaev and D. Loss, Phys. Rev. B **71**, 205324 (2005); M. Florescu and P. Hawrylak, *ibid.* **73**, 045304 (2006); J. I. Climente, A. Bertoni, G. Goldoni, M. Rontani, and E. Molinari, *ibid.* **76**, 085305(R) (2007); M. Prada, R. H. Blick, and R. Joynt, *ibid.* **77**, 115438 (2008).
[16] T. Bergsten, T. Kobayashi, Y. Sekine, and J. Nitta, Phys. Rev. Lett. **97**, 196803 (2006).
[17] M. F. Borunda, X. Liu, A. A. Kovalev, X. J. Liu, T. Jungwirth, and J. Sinova, Phys. Rev. B **78**, 245315 (2008).
[18] D. Frustaglia and K. Richter, Phys. Rev. B **69**, 235310 (2004).
[19] O. Kalman, P. Földi, M. G. Benedict, and F. M. Peeters, Phys. Rev. B **78**, 125306 (2008).
[20] R. Citro and F. Romeo, Phys. Rev. B **75**, 073306 (2007).
[21] U. Aeberhard, K. Wakabayashi, and M. Sigrist, Phys. Rev. B **72**, 075328 (2005).
[22] K. Niemelä, P. Pietiläinen, P. Hyvönen, and T. Chakraborty, Europhys. Lett. **36**, 533 (1996).
[23] J. I. Climente, J. Planelles, and W. Jaskólski, Phys. Rev. B **68**, 075307 (2003).
[24] A. Puente, L. Serra, and R. G. Nazmitdinov, Phys. Rev. B **69**, 125315 (2004).
[25] S. Viefers, P. Koskinen, P. Singa Deo, and M. Manninen, Physica E (Amsterdam) **21**, 1 (2004).
[26] T. Chakraborty and P. Pietiläinen, Phys. Rev. B **50**, 8460 (1994).
[27] A. O. Govorov, S. E. Ulloa, K. Karrai, and R. J. Warburton, Phys. Rev. B **66**, 081309(R) (2002).
[28] J. I. Climente, J. Planelles, and J. L. Movilla, Phys. Rev. B **70**, 081301(R) (2004).
[29] Y. V. Pershin and C. Piermarocchi, Phys. Rev. B **72**, 125348 (2005).
[30] V. M. Fomin, V. N. Gladilin, S. N. Klimin, J. T. Devreese, N. A. J. M. Kleemans, and P. M. Koenraad, Phys. Rev. B **76**, 235320 (2007).
[31] V. M. Fomin, V. N. Gladilin, J. T. Devreese, N. A. J. M. Kleemans, and P. M. Koenraad, Phys. Rev. B **77**, 205326 (2008).
[32] N. A. J. M. Kleemans, I. M. A. Bominaar-Silkens, V. M. Fomin, V. N. Gladilin, D. Granados, A. G. Taboada, J. M. Garcia, P. Offermans, U. Zeitler, P. C. M. Christianen, J. C. Maan, J. T. Devreese, and P. M. Koenraad, Phys. Rev. Lett. **99**, 146808 (2007).
[33] J. Splettstoesser, M. Governale, and U. Zülicke, Phys. Rev. B **68**, 165341 (2003).
[34] J. S. Sheng and K. Chang, Phys. Rev. B **74**, 235315 (2006).
[35] G. H. Ding and B. Dong, Phys. Rev. B **76**, 125301 (2007).
[36] Q. F. Sun, X. C. Xie, and J. Wang, Phys. Rev. Lett. **98**, 196801 (2007).
[37] G. Y. Huang and S. D. Liang, EPL **86**, 67009 (2009).
[38] A. G. Aronov and Y. B. Lyanda-Geller, Phys. Rev. Lett. **70**, 343 (1993).
[39] F. E. Meijer, A. F. Morpurgo, and T. M. Klapwijk, Phys. Rev. B **66**, 033107 (2002).
[40] S.-R. Eric Yang, Phys. Rev. B **74**, 075315 (2006).
[41] J. D. Koralek, C. Weber, J. Orenstein, A. Bernevig, S. Zhang, S. Mack, and D. Awschalom, Nature (London) **458**, 610 (2009).
[42] B. A. Bernevig, J. Orenstein, and S. C. Zhang, Phys. Rev. Lett. **97**, 236601 (2006).
[43] A. Lorke, R. J. Luyken, A. O. Govorov, J. P. Kotthaus, J. M. Garcia, and P. M. Petroff, Phys. Rev. Lett. **84**, 2223 (2000).
[44] W. Knap, C. Skierbiszewski, A. Zduniak, E. Litwin-Staszewska,

D. Bertho, F. Kobbi, J. L. Robert, G. E. Pikus, F. G. Pikus, S. V. Iordanskii, V. Mosser, K. Zekentes, and Yu. B. Lyanda-Geller, Phys. Rev. B **53**, 3912 (1996).

[45] S. Saikin, M. Shen, M. C. Cheng, and V. Privman, J. Appl. Phys. **94**, 1769 (2003).

[46] M. J. Snelling, E. Blackwood, C. J. McDonagh, R. T. Harley, and C. T. B. Foxon, Phys. Rev. B **45**, 3922 (1992).

[47] M. Bayer, M. Korkusinski, P. Hawrylak, T. Gutbrod, M. Michel, and A. Forchel, Phys. Rev. Lett. **90**, 186801 (2003).

[48] T. Chwiej and B. Szafran, Phys. Rev. B **78**, 245306 (2008).

[49] For $\alpha=\beta$ and $g=0$ each energy level is twofold degenerate with respect to the *s* parity. The degenerate states corresponding to even and odd *s* parities have the same charge densities, and the spin-up and spin-down densities are exchanged.

[50] The eigenstates of $\sigma_x-\sigma_y$ can be constructed from the odd and the even s-parity eigenstates which in the case of $\alpha=\beta$ and $g=0$ correspond to degenerate energy levels. The eigenstates of $\sigma_x-\sigma_y$ are no longer *s*-parity eigenstates.

[51] B. Szafran, M. P. Nowak, S. Bednarek, T. Chwiej, and F. M. Peeters, Phys. Rev. B **79**, 235303 (2009).

[52] T. Chwiej and B. Szafran, Phys. Rev. B **79**, 085305 (2009).

[53] Figure 2 presents the case of pure Rashba coupling and $g=0$. For the pure Dresselhaus coupling the energy spectrum is identical, the average *z* component of the spin and the *s* parity are inverted.